State of Oregon
Department of Geology and Mineral Industries
John D. Beaulieu, State Geologist

Geological Map Series

GMS–114

Text

Geologic Map of the Imbler Quadrangle, Union County, Oregon

by

Mark L. Ferns, Vicki S. McConnell, and Ian P. Madin,

Oregon Department of Geology and Mineral Industries

and

J. Van Tassell, Eastern Oregon University

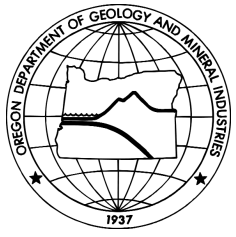

2002

Contents

Figures

Tables

Oregon Department of Geology and Mineral Industries Geological Map Series, ISSN 0278-3703
Published in conformance with ORS 516.030

For copies of this publication or other information about Oregon's geology and natural resources, contact:

Nature of the Northwest Information Center
800 NE Oregon Street #5
Portland, Oregon 97232
(503) 872-2750
http://www.naturenw.org

INTRODUCTION

The Imbler 7½-minute quadrangle is located in the north-central part of the Blue Mountains Province of northeastern Oregon, just northeast of La Grande, Oregon (Figure 1). The quadrangle covers the northern end of the Grande Ronde Valley and includes the city of Imbler.

Major topographic features include the floor and eastern escarpment of the Grande Ronde Valley, one of the most prominent structural depressions in northeast Oregon. The valley's eastern escarpment rises nearly 800 m above the valley floor; elevations in the quadrangle range from 1,636 m at the top of the Mount Harris volcano to 786 m where the Grande Ronde River exits the valley in the northeast corner of the quadrangle. The City of Imbler is located on the east flank of Sand Ridge (Figure 2), a broad, central highland made up of low-relief rolling hills. Sand Ridge stands 10–30 m above the adjoining channel and flood plains of the Grande Ronde River on the east and Willow Creek on the west. The Grande Ronde River enters the Imbler

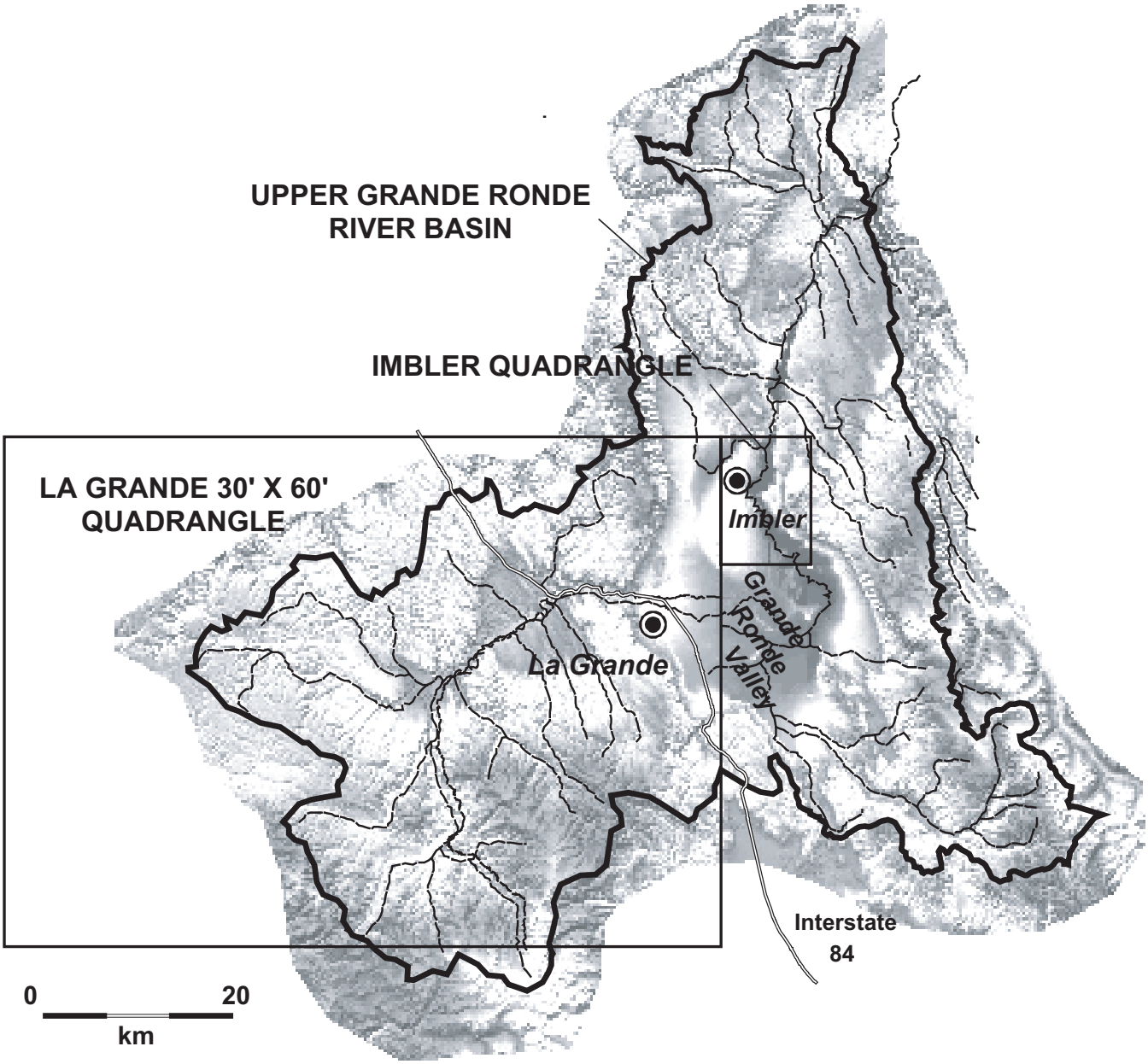

Figure 1. Shaded-relief map of the Grande Ronde Valley, showing the Imbler 7½-minute quadrangle and the La Grande 30×60-minute quadrangle (Ferns and others, 2001). The upper Grande Ronde River basin is outlined in bold.

quadrangle along the foot of the eastern escarpment. Following a tortuously meandering course, the river swings from a general northwest trend to a northeast trend at the foot of Mount Harris, dropping about 2 m in elevation over a river channel distance of over 43 km. Mint, grass seed, and alfalfa are the major crops raised on the intensely cultivated valley floor. Uplands are used for grazing and timber harvest. All of the land in the quadrangle is privately owned.

The 1:24,000-scale geologic map of the Imbler quadrangle was partially funded by the U.S. Geological Survey (USGS) National Cooperative Geologic Mapping Program under assistance award no.99HQAG0036. The map is released as an interim product as part of a larger mapping project covering the entire upper Grande Ronde River basin (Figure 1).

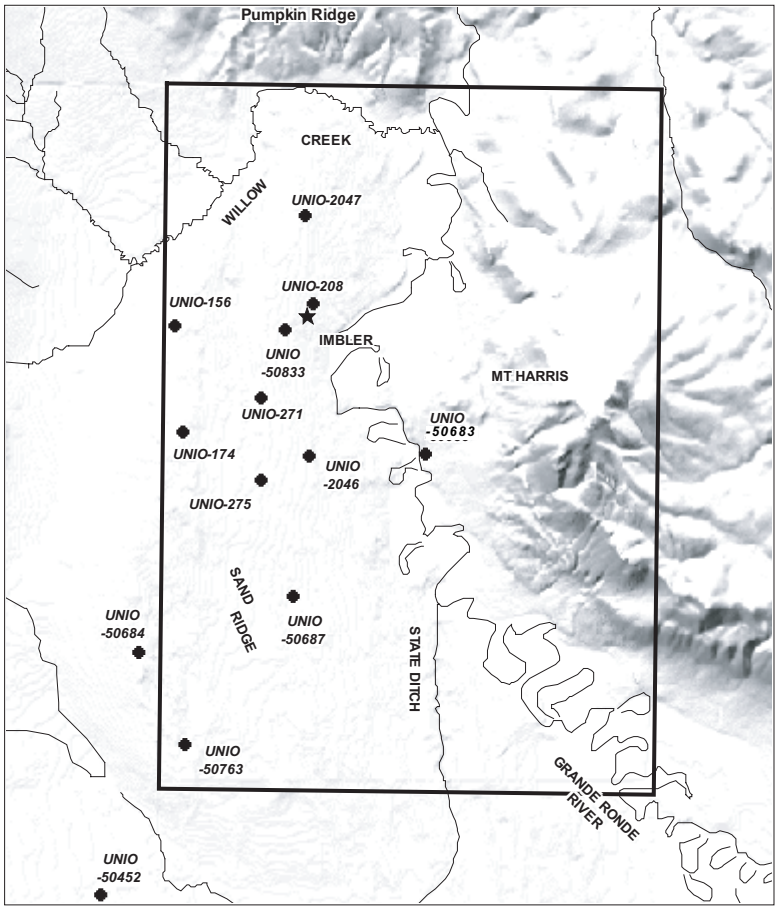

Figure 2. Location of deep water wells in and adjacent to the Imbler quadrangle. Wells identified by Oregon Water Resources Department ID numbers. Note the tortuously meandering course of the Grande Ronde River as it enters the southeastern corner of the quadrangle. Much of the flow from the Grande Ronde River currently bypasses the meanders through the State Ditch.

METHODOLOGY AND PREVIOUS WORK

Geologic data were collected at the scale of 1:24,000 and combine new mapping with published and unpublished data from air photos, orthophotoquads, and digital shaded-relief images derived from USGS 30-m DEM (Digital Elevation Model) grids. Mapping was supplemented with X-ray fluourescence (XRF) geochemical analyses and $^{40}Ar/^{39}Ar$ radiometric age determinations.

Subsurface geology in cross sections is based on analyses of water-well drill cuttings from six recently drilled deep-water wells in the north end of the Grande Ronde Valley (Figure 2). Analytical data were supplemented by interpretation of water-well drill logs from older wells. A partial ground magnetic survey was conducted in the southern part of the quadrangle with a proton precession magnetometer.

Comparatively few geologic studies have been done in the Imbler quadrangle. The quadrangle was first mapped in the late 1950s by Hampton and Brown (1964), who produced a generalized 1:62,500-scale map of the Grande Ronde Valley. Walker (1979) later produced a 1:250,000-scale map for the Oregon part of the Grangeville quadrangle that placed Mount Harris volcano in the Columbia River Basalt Group, even though earlier workers (Hampton and Brown, 1964) recognized that andesite lava flows on Mount Harris differed from typical Columbia River Basalt lava flows. The Mount Harris volcano was first described as a possible, post-Columbia River basalt, eruptive center by White (1981). White (1981) and Gehrels (1981) were the first to describe the structural framework of the Grande Ronde Valley in detail. Later studies in and adjacent to the quadrangle include Personius (1998), Ferns and Madin (1999), and Ferns and others (in preparation).

DESCRIPTION OF MAP UNITS

Surficial Deposits

Qa **Stream alluvium (Holocene and upper Pleistocene)**—Gravel, sand, and silt deposited in active stream channels and on adjoining flood plains. Unit includes gravel and channel sand deposited in active or recently abandoned channels and overbank silt and mud deposited in the modern Grande Ronde River flood plain

Qal **Alluvial plain deposits (Holocene? and upper Pleistocene)**—Mainly black silt, clay, and sand deposited in the alluvial plain of Willow Creek. Unit includes minor lenses of pebbly, coarse- to medium-grained sand, and organic and diatomite-rich clays. Unit is interpreted as marsh, slow-moving stream, and shallow lake deposits

Qfs **Talus, scree, and debris-flow deposits (Holocene and Pleistocene)**—Coarse, unconsolidated breccias made up of andesite and dacite blocks as much as 3 m in diameter that were deposited by rock falls and small debris avalanches. Multiple-age deposits include young andesite and dacite boulder fields and older soil-covered colluvial wedges. Unit includes debris-flow deposits near the foot of Mount Harris, on Hull Lane

Qf **Alluvial fan deposits (Holocene and Pleistocene)**—Mainly unconsolidated, poorly sorted deposits of coarse boulder gravel, gravel, and sand deposited along the south and west flanks of Mount Harris. Unit consists mainly of coarse-grained, poorly sorted boulder gravels. Upper slopes include unstable colluvial wedges of intermixed soil and rock that mantle fault contacts. Unit includes fine to medium gravels in the southeast corner of the quadrangle that form part of an extensive series of coalescing alluvial fans extending southeast along the face of the eastern escarpment

Qe **Eolian sand and loess (Holocene and upper Pleistocene)**—Windblown deposits of medium- to fine-grained sand and loess. Unit forms the Sand Ridge (Figure 2), a stabilized and extensively cultivated, north-trending, longitudinal dune field that stands 10–30 m above the modern flood plain and covers most of the west half of the quadrangle. Closed depressions between the old dune crests are marked by ephemeral ponds and bogs. Well logs indicate that the windblown sand is no more than 20 m thick on Sand Ridge. Along the northern margin of the quadrangle, the unit also includes thin (<5 m) accumulations of fine silt (loess) that extend into the Elgin quadrangle and mantle much of the south slope of Pumpkin Ridge

Qls **Landslide deposits (Holocene and Pleistocene)**—Unconsolidated, chaotically mixed masses of rock and soil. Landforms typified by sloping, hummocky surfaces marked by closed depressions, springs and wet seeps, scarps, cracks, and crevices. Unit locally includes rockfall, mudflow and debris-flow deposits. The massive debris-flow deposit at the foot of Mount Harris at Grays Corner (southwest corner, sec. 2, T. 2 S., R. 39 E.) contains large (10-m diameter) blocks of dacite. The large composite slide mass off the south flank of Mount Harris on the Mount Harris Loop road is fed by massive rock falls of dacite and andesite. Older slides are mantled by fan alluvium, loess, and ash

Qts **Terrace deposits (Pleistocene)**—Gravel and sand. Unit includes poorly consolidated deposits of coarse pebbly sand and medium- to fine-grained sand in the south end of the quadrangle and coarse boulder gravels in the northeast of the quadrangle. Terrace deposits exposed in the south end of the quadrangle

are erosional remnants of a somewhat sinuous body of gravelly sand that stands 5–10 m above the modern valley floor. These remnants are interpreted by Ferns and others (in preparation) as surficial sand levee deposits that mark the high stand of the valley fill sediments (unit QTal). Coarse boulder gravels in the northeast corner of the quadrangle are part of an extensive sheet of outwash gravels deposited by Indian Creek

Subsurface Sedimentary Deposits

QTal **Lacustrine and fluvial sediments (Pleistocene, Pliocene, and Miocene)**—Mainly fine silt, but locally includes sand, fine gravel, diatomite, tuff, and organic-rich black clays. Unit includes all sedimentary fill deposits in the Grande Ronde Valley that underlie the surficial units. Water wells indicate that unit thickens southward from about 150 m at Imbler to as much as 900 m south of Alicel (Figure 2 and Table 3). Detailed stratigraphy is based on cuttings from four recently drilled water wells, the deepest of which was drilled for Greg Bingaman in 1998 (Oregon Water Resources Department [OWRD] no. UNIO-50684). A thickness of 595 m of unit QTal sediments was penetrated by this well, which is situated 0.3 km west of the quadrangle boundary in the Summerville quadrangle. A newer well was drilled for Ross Bingaman in 2000 just west of Imbler (OWRD no. UNIO-50833) and penetrated 141 m of unit QTal. The basal part of the unit in both wells is marked by a 5- to 10-m-thick sequence of organic-rich, fossiliferous, brown clays and silts. The well UNIO-50684 coarsens upward into a 280-m-thick section of sandy silt interbedded with thin seams of gravel and sand. Lower gravels and sands at both wells are dominated by arkosic sands that contain clasts of pre-Tertiary rocks. Detrital clasts of Tertiary volcanic rocks have not been identified in the lower one-third of the section at both wells. Late Miocene fish fossils, including a catfish, *Ameiurus* cf. *A. reticulatus*, as well as a sunfish and an unidentified minnow have been recovered from the base of the sedimentary section in the well UNIO-50833 (Van Tassell and others, 2001). A water-laid ash recovered at a depth of 473 m below land surface in the deeper well UNIO-50684 yielded a $^{40}Ar/^{39}Ar$ isochron age of 7.5±0.1 Ma (sample 98BI1553, Table 1). The dated ash sample is a rhyolite with 72.69 weight percent SiO_2, 16.08 weight percent Al_2O_3, and 2.91 weight percent K_2O (Table 2). An overlying ash sample collected from a depth of 458 m is also a rhyolite, with 71.15 weight percent SiO_2, 17.90 weight percent Al_2O_3, and 2.06 weight percent K_2O (sample 98BI1502, Table 2). The overlying ash displays an unusual trace-element pattern with 112 ppm yttrium (Y) and 47.6 ppm niobium (Nb). The upper 200 m of section in the well UNIO-50684 is made up mostly of sandy silt with thin (<3 m) seams of sand and gravel that tentatively correlate with dated sediments from another well that is located 2.5 km to the southwest in the adjacent La Grande quadrangle (well UNIO-50452, Figure 2 and Table 3). A water-laid ash collected from a depth of 108 m in this well yielded a $^{40}Ar/^{39}Ar$ radiometric age of 3.1±0.3 Ma (sample Terry-356, Table 1) (Van Tassell and others, 2001)

Tme **Sedimentary interbed (middle Miocene)**—Unconsolidated to poorly consolidated tuffaceous sand and volcanic clast gravels in secs. 13 and 14, T. 1 S., R. 39 E., on the lower northeast flank of Mount Harris. Unit is not exposed in outcrop, mapped on basis of rounded float and intermixed angular fragments of tuffaceous sandstone in disturbed ground. Unit appears to overlie a 10.85-Ma basanite lava flow (unit Tpgh) and banks up against the basal Mount Harris lava flows (unit Tgha). Unit is tentatively correlated with more extensive tuffaceous sedimentary interbeds that are exposed between lavas of the informally named Elgin volcanic complex (discussed below) and underlying olivine basalt flows of the lavas of Glass Hill in the Elgin quadrangle to the north

Table 1. $^{40}Ar/^{39}$ Ar age determinations. Plateau ages derived from incremental fusion. QTal ashes are from well cuttings at 356 and 1,553 ft depth, respectively.

Sample no.	Rock type	Map unit	Age (Ma)	Notes
Terry-356	Rhyolite ash	QTal	3.1 ± 0.3	Well UNIO-50452, Figure 2 (La Grande quadrangle)
98BI1553	Rhyolite ash	QTal	7.5 ± 0.1	Well UNIO-50684, Figure 2, (Summerville quadrangle)
Rockwall	Andesite	Tpea	10.4 ± 0.9	Sample from Partridge Creek quadrangle
99-LCC98	Dacite	Tpgd	11.8 ± 0.09	Sample from Mount Fanny quadrangle
99-LCC114	Basanite	Tpgh	10.8 ± 0.18	Sample from Mount Fanny quadrangle
99-LG-59	Dacite	Tghp	11.9 ± 0.12	Map no. 5, Table 2, Imbler quadrangle

Volcanic Rocks

Whole-rock chemical data are useful in classifying volcanic rocks, as many lavas are too fine grained and glassy to be adequately characterized by mineralogical criteria alone. Rock names, e.g., basalt or basaltic andesite, are derived from the total alkalis versus silica (TAS) diagram of Le Maitre and others (1989) (Figure 3). Chemical data can be useful in determining evolutionary links between successive lava flows. Various diagrams that show the relative role of iron enrichment in volcanic processes are commonly used to separate "tholeiitic" lavas from"calc-alkalic" lavas (Figures 4 and 5). These distinctions are particularly useful in separating the predominantly tholeiitic Columbia River Basalt Group lavas from the predominantly calc-alkalic lavas of the Powder River Volcanic Field (Figures 4 and 5)

Powder River Volcanic Field (upper Pliocene to middle Miocene)— Following Bailey (1990), Hooper and Swanson (1990), and Ferns and others (2001), we have applied the name "Powder River Volcanic Field" to the entire sequence of compositionally diverse, geographically restricted, predominantly calc-alkalic and alkaline lavas that crop out between Baker City and Elgin. In this region, the Powder River Volcanic Field includes all lavas erupted after the last eruption of Grande Ronde Basalt Group flood basalts. As such, the Powder River Volcanic Field includes lavas ranging in age from 3.1 to 14.3 Ma (late Pliocene to middle Miocene) (Ferns and others, 2001). In the Imbler quadrangle, the Powder River Volcanic Field includes the lavas of Elgin (units Tpea, Tpeb), the distal edge of a basanite lava flow (unit Tpgh) exposed in the northeast corner of the quadangle, the lavas of Mount Harris (units Tghd, Tghp, Tghi, and Tgha), and a basal sequence of dacite (unit Tpgd), andesite (unit Tpga), and olivine basalt (unit Tpgb) lava flows. The basanite lava flow, the lavas of Mount Harris, and the underlying lavas are considered to be part of the lavas of Glass Hill, as defined by Ferns and others (2001)

Lavas of Elgin (Pliocene? or upper Miocene)— Lava flows produced by a complex of small shield volcanos extending through the center of the Elgin quadrangle to the north and clustered about the town of Elgin (Figure 6). These are for the most part hornblende-phyric lavas that form low shield volcanoes typically between 2 and 4 km in diameter and <150 m in height. Lavas include trachybasalt and trachyandesite and typically contain high levels (>1,000 ppm) of strontium. Chemically and petrographically similar lavas originated from a string of small, 7.3- to 6.5-Ma volcanoes on the plateau west of the Grande Ronde Valley and were described as the Sugarloaf Mountain Volcanics by Kienle and others (1979) and the lavas of Sugarloaf Mountain by Ferns and others (2001). In the Imbler quadrangle, mapped units of the lavas of Elgin include the following:

Tpea **Trachyandesite and andesite (Pliocene? or upper Miocene)—** Light bluish gray to gray, aphyric andesite and trachyandesite flows that crop out low on the north flank of Mount Harris. Typically very

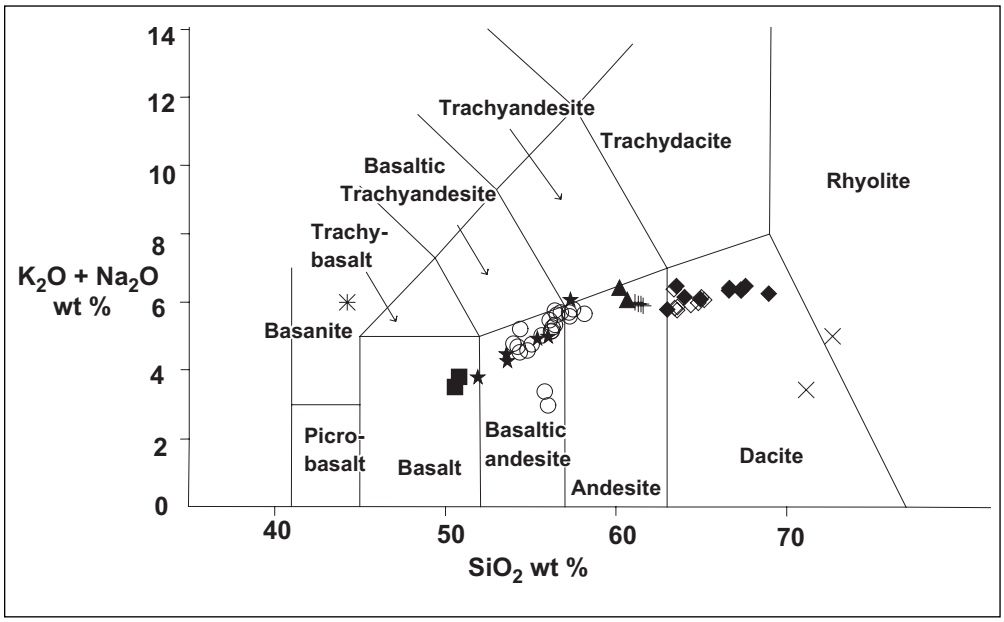

Figure 3. TAS (total alkalis vs. silica) plot of Le Maitre and others (1989) for selectedvolcanic rocks from Table 2. × = Map unit QTal rhyolite ash; filled triangles = Elgin lavas; asterisk = Bell-tone basanite; filled diamonds = Mount Harris lavas; open diamonds = other Glass Hill andesites and dacites; open circles = other Glass Hill andesites and basaltic andesites; filled squares = Glass Hill basalt; filled stars = Grande Ronde Basalt.

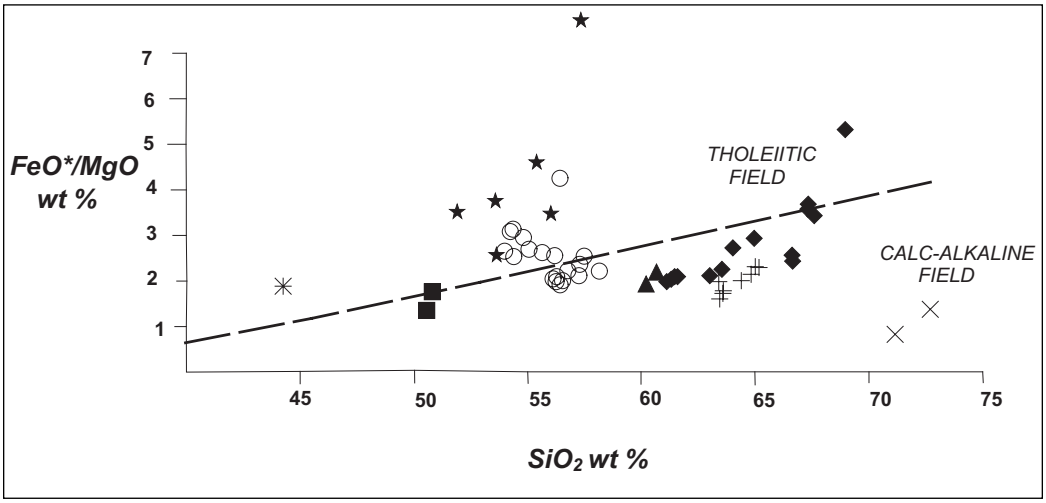

Figure 4. FeO*/MgO vs. SiO_2 plot of Miyashiro (1974) for selected volcanic rocks from Table 2. Symbols as in Figure 3.

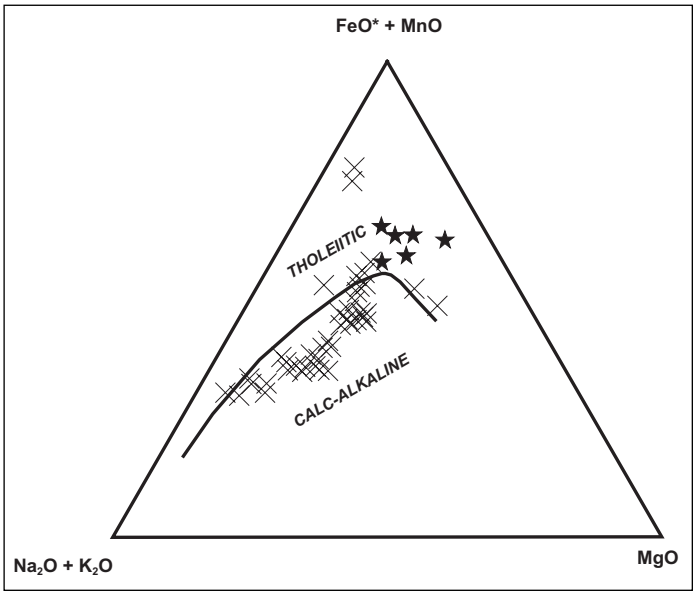

Figure 5. AFM plot of selected volcanic rocks from Table 2. × = Powder River Volcanic Field units; filled stars = Columbia River Basalt Group units. Curved line separating tholeiitic and calc-alkaline fields from Kuno (1968).

fine grained with pronounced flow foliation. In thin section, marked by fine-grained pilotaxitic groundmass composed of a mat of aligned, needle-shaped plagioclase crystals that wrap around rotated and partially resorbed orthopyroxene microphenocrysts. Analyses of two samples from the Imbler quadrangle (nos. 99-LG-76 and 99-LG-78, Table 2) ranged from 60.21 to 60.67 weight percent SiO_2; 17.83 to 18.43 weight percent Al_2O_3; 1.44 to 1.85 weight percent K_2O; 4.59 to 4.63 weight percent Na_2O; and 1,068 to 1,082 ppm Sr. Chemically and petrographically similar lavas form small shield volcanoes in the Elgin quadrangle immediately to the north. A sample (Rockwall, Table 1) from one of the Elgin shield volcanoes yielded a poor $^{40}Ar/^{39}Ar$ plateau whole-rock age of 10.4±0.9 Ma and a poor isochron age of 5.7±0.9 Ma. The sample yielded excess argon, likely due to fine-grained groundmass alteration products. This flow is no older than 10.4±0.9 Ma and may be as young as 5.7±0.9 Ma

Tpeb **Basaltic trachyandesite and trachyandesite (Pliocene? or upper Miocene)**—Light bluish gray to gray, fine-grained basaltic trachyandesite and trachyandesite flows. Nearly all flows contain scattered black amphibole phenocrysts. In the Imbler quadrangle, unit includes the distal edges of the coalescing lava flows that, in the Elgin quadrangle to the north, form the south and east flanks of Pumpkin Ridge. These are gray to bluish-gray, open-textured flows that contain scattered black amphibole phenocrysts. In thin section, the relict amphibole phenocrysts are usually replaced by opaque iron oxides. The oxide masses are sometimes rimmed or cored by small clinopyroxene crystals. Individual flows are commonly trachytic, with green clinopyroxene and, more rarely, plagioclase phenocrysts as much as 3 mm in length. A representative analysis of a basaltic trachyandesite on the south end of Pumpkin Ridge in the Elgin quadrangle yielded 53.95 weight percent SiO_2; 17.01 weight percent Al_2O_3; 1.61 weight percent TiO_2; 1.80 weight percent K_2O; 5.17 weight percent Na_2O; and 2,311 ppm Sr

Lavas of Glass Hill (upper and middle Miocene)—The more than 650 m of middle Miocene calc-alkalic and alkaline lava flows that are exposed along the eastern escarpment of the Grande Ronde Valley make up the lavas of Glass Hill as defined by Ferns and others (2001). The base of the formation is marked by high-alumina olivine basalt flows that are overlain by basaltic andesite, andesite, dacite, and alkali olivine basalt and basanite flows. Mapped units in the Imbler quadrangle include the Bell-tone basanite, the flows that make up the Mount Harris volcano, and underlying andesite, dacite, and olivine basalt flows

Tpgh **Bell-tone basanite (upper or middle Miocene)**—Glassy, dark-gray to black, massive, olivine-phyric lava flow that is exposed in secs. 12 and 13, T. 1 S., R. 39 E. Unit is typically jet black on fresh surfaces and breaks with conchoidal fractures. Weathered surfaces typically bluish gray or red. The rock contains abundant clear, yellow olivine crystals as much as 2 mm in diameter. Lava is phonolitic, ringing like a bell when struck by a hammer. Unit is exposed only east of Mount Harris, where a single flow about 14 m thick is overlain by a trachyandesite flow (unit Tpea). The basanite flow rests here directly on olivine basalt (unit Tpgb). The basanite flow is partly separated from flanking basal Mount Harris flows (unit Tgha) by a thin sedimentary unit (unit Tme). In thin section, the basanite typically contains as much as 10 percent euhedral olivine crystals and 7 percent iron/titanium oxides. Olivine phenocrysts are as much as 2 mm in diameter and set in a microcrystalline groundmass of intersertal to intergranular plagioclase, FeTi oxides, and clinopyroxene. Distinguished chemically by low silica (45.58 weight percent SiO_2) and high soda (5.26 weight percent Na_2O) content (sample 99-LG-72, Table 2). A sample of the basanite yielded a plateau $^{40}Ar/^{39}Ar$ age of 10.85±0.18 Ma (sample 99-LCC114, Table 1). A similar lava flow to the east has been dated at about 11.6 Ma (Fiebelkorn and others, 1983)

Lavas of Mount Harris (middle Miocene)—Includes all lava flows, domes, and plugs that make up the Mount Harris volcano. Lavas range in composition from high-silica andesite to dacite

Tghd **Dacite, undivided (middle Miocene)**—Massive light-gray to light bluish- and light pinkish gray lava flows that cap the upper flanks of Mount Harris. Unit includes at least two separate flows; both are nearly aphyric, <1 percent microphenocrysts. In thin section, marked by pronounced, fine-grained pilotaxitic texture enclosing small (<1 mm diameter) orthopyroxene or clinopyroxene microphenocrysts. Analyses of three samples (sample nos. 98MAD198, 99-LG-41, and 98MAD177, Table 2) ranged from 64.02 to 67.33 weight percent SiO_2, 16.47 to 17.021 weight percent Al_2O_3, 1.64 to 1.84 weight percent K_2O, 4.31 to 4.51 weight percent Na_2O, and 640 to 685 ppm Sr

Tghp **Dacite plug (middle Miocene)**—Massive, light-gray to light bluish gray and light pinkish gray lava that forms a 120-m-high central plug at the summit of Mount Harris. The dacite is fine grained in thin section, with plagioclase and heavily altered, oxide rimmed hornblende phenocrysts as much as 2 mm in length. Marked by a crytpocrystalline to very fine grained pilotaxitic groundmass. Analyses of three samples (sample nos. 99-LG-59, 98MAD179, and 99-VLG-16, Table 2) ranged from 66.62 to 68.95 weight percent SiO_2; 16.46 to 16.66 weight percent Al_2O_3; 1.74 to 1.80 weight percent K_2O; 4.45 to 4.74 weight percent Na_2O, and 618 to 769 ppm Sr. The plug has yielded a $^{40}Ar/^{39}Ar$ plateau age of 11.9±0.12 Ma (sample 99-LG-59, Table 1)

Tghi **Dacite dome (middle Miocene)**—Massive, gray to bluish-gray lava that forms a small dome on the southwest flank of Mount Harris. Nearly aphyric, with <1 percent clinopyroxene and partially resorbed, zoned plagioclase phenocrysts. The clinopyroxene occurs in glomeroporphyritic clots. A sample (sample no. 99-LG-79, Table 2) gave a geochemical analysis of 63.54 weight percent SiO_2, 16.39 weight percent Al_2O_3, 1.87 weight percent K_2O, 4.61 weight percent Na_2O, and 1,021 ppm Sr. Contact relationships are unclear, but unit appears to be a large dacite dome that is partially intrusive

Tgha **Andesite and dacite (middle Miocene)**—Dark grayish black to black, glassy, high-silica andesite and dacite lava flows. Typically weathering red and marked by vesiculated flow tops. The rock breaks with conchoidal fractures. Flow-on-flow sequence with an aggregate thickness of at least 180 m. Unit includes pilotaxitic and hyalophitic flows that contain orthopyroxene microphenocrysts. Hyalophitic flows are marked by small blocky plagioclase phenocrysts set in an oxide-rich glassy groundmass. Five samples from flows around Mount Harris (sample nos. 99-LG-43, 98MAD169, 98MAD175, 98MAD1745, and 98MAD173, Table 2) ranged from 61.11 to 63.0 weight percent SiO_2, 16.43 to 16.57 weight percent Al_2O_3, 1.89 to 2.11 weight percent K_2O, 3.85 to 4.01 weight percent Na_2O; and 520 to 546 ppm Sr

Tpgd **Dacite (middle Miocene)**—Light bluish gray to light pinkish gray, dacite lava flows. Flow-on-flow sequence exposed beneath the andesite and dacite flows (unit Tgha) on the southern flanks of Mount Harris. Lavas are fine grained and aphyric. In thin section, marked by pilotaxitic texture with rare clinopyroxene and orthopyroxene microphenocrysts. According to geochemical characteristics, unit is also present in wells UNIO-50683 and UNIO-50687 (samples IM-1-1011 and SV51-1132; -1198; -1274; -1365; and -1444, Table 2, map locations 17 and 18, respectively). Analytic results from these samples and samples 98MAD171 (map location 14) and 99-LG-82 (map location 15) ranged from 63.40 to 65.17 weight percent SiO_2, 16.26 to 16.89 weight percent Al_2O_3, 1.60 to 1.78 weight percent K_2O, 3.99 to 4.61 weight percent Na_2O, and 654 to 916 ppm Sr. The dacite unit in the UNIO-50687 well is more than 100 m thick

Tpga **Basaltic andesite and andesite (middle Miocene)** (shown in cross section only)—Flow-on-flow sequence of vesicular, glassy, aphyric basaltic andesite and andesite flows. Although this unit is not exposed in the quadrangle, it is penetrated by water wells in the Grande Ronde Valley. Petrographic and lithologic descriptions are of samples collected from outside the quadrangle. Mainly platy-jointed, aphyric glassy andesite flows. Includes black, glassy lavas and light- to medium-gray, finely crystalline lavas. In thin section, characterized by altered olivine phenocrysts and small pyroxene and plagioclase microphenocrysts set in a very fine grained pilotaxitic groundmass. Analyzed samples from water-well drill cuttings (sample IM-1-1137 from well UNIO-50683, map location 17, and nine samples from well UNIO-50687, map location 18,) are basaltic andesite and andesite with 54.36–58.15 weight percent SiO_2, 17.26–20.56 weight percent Al_2O_3, 0.98–1.57 weight percent K_2O, 278–690 ppm Sr, and 20–25 ppm Nb (Table 2). Although most flows show calc-alkalic affinities (Figures 4 and 5), flows in the upper part of the well UNIO-50684 (outside the Imbler quadrangle) have unusually high alumina contents (17–21 weight percent Al_2O_3) and are tholeiitic. Individual flows exposed outside the quadrangle are as much as 50 m thick. As indicated by water-well stratigraphy, the unit thins from 150 m in the southern part of the valley to 40 m at Imbler. In its chemical characteristics, the unit is equivalent to the basalt of Ramo Flat (Ferns and others, in preparation) a series of small basaltic andesite lava flows that are associated with small, deeply eroded cinder cones south of Union. Also chemically equivalent to the high-Niobium andesites of Bailey (1990), a sample of which yielded a $^{40}Ar/^{39}Ar$ age of 13.0±0.1 Ma

Tpgb **Olivine basalt (middle Miocene)**—Flow-on-flow sequence of vesicular holocrystalline olivine basalt flows. Generally gray or light gray and weathering to compact rounded boulders in a granular soil. Commonly characterized by a diktytaxitic texture where olivine phenocrysts as much as 3 mm in diameter are set in an open-textured groundmass of coarse plagioclase laths. Includes dark-gray, glassy lavas with yellow-green olivine phenocrysts. Individual basalt flows are typically 5–14 m thick. As indicated by water-well cuttings from the City of Imbler well (Unio-208), unit thickness is as much as 150 m in the northern part of the Grande Ronde Valley. Flow compositions range from 47 to 53 weight percent SiO_2 and from 15.21 to 17.27 weight percent Al_2O_3. According to M.H. Beeson, Portland State University (unpublished data), analyses from water-well cuttings show that the map unit includes at least three chemically distinctive flow packages: a low-potassium, low-titanium variant (<0.5 weight percent K_2O, <1.2 weight percent TiO_2); a moderate-potassium, moderate-titanium variant (0.5–0.8 weight percent K_2O, ~2.0 weight percent TiO_2); and a high-titanium, moderate-potassium variant (~2.5 weight percent TiO_2, 0.5–0.8 weight percent K_2O). In the northeast corner of the Imbler quadrangle, unit thins and, in places, is marked by pillow basalts, and its flows directly overlie palagonite breccias (unit Tcgv). Elsewhere along the margins of the Grande Ronde Valley the olivine basalt flows are separated from underlying Grande Ronde Basalt by thin layers of tuffaceous sediments, ash-flow tuff, or cobble gravels (e.g., Summerville quadrangle, Ferns and Madin, 1999). Where overlain by dacite lava flows (unit Tpgd), this unit has the tendency to form large landslides. Lowermost flows have reversely polarized thermal remanent magnetization, while uppermost flows are of normal polarity. Middle Miocene age based on whole-rock $^{40}Ar/^{39}Ar$ ages of 13.3±0.8; 13.7±0.1 and 14.4±0.2 Ma for similar olivine basalt flows to the east (Bailey, 1990). Equivalent to the diktytaxitic phase of the basalt of Glass Hill of Barrash and others (1980)

Columbia River Basalt Group (middle and lower Miocene)—The Grande Ronde Basalt is the only Columbia River Basalt Group formation exposed in the Imbler quadrangle. Although both of the younger Wanapum Basalt and Saddle Mountains Basalt are exposed only a short distance to the north in the Elgin quadrangle, neither formation has been identified within the Grande Ronde Valley

Tcg **Grande Ronde Basalt, undivided (middle Miocene)** (shown in cross section only)—Flow-on-flow sequence of bluish-black, aphyric to sparsely plagioclase-phyric lava flows shown in the cross sections. Although the unit includes the N2, R2, N1, and R1 magnetostratigraphic units of Reidel and others (1989), analyzed samples from the Imbler well (Beeson, unpublished data) indicate that wells in the valley have not penetrated beyond the upper part of the R2 magnetostratigraphic unit (Reidel and others, 1996). Exposures along escarpments bordering the valley west and south of the Imbler quadrangle show unit to be as much as 650 m thick

Tcgn2 **N2 Grande Ronde Basalt (middle Miocene)**—Flow-on-flow sequence of bluish-black, aphyric to sparsely plagioclase-phyric lava flows. Includes both holocrystalline and glassy lavas that weather to form steep slopes. Generally weathers to orange-brown, angular blocks. Fresh hand samples are generally aphyric and range in color from bluish gray to black. Individual lava flows are thin (<15 m) with conspicuous vesicular flow tops and basal flow breccias. In thin section, typically sparsely plagioclase phyric, containing scattered plagioclase phenocrysts as much as 2 mm in length and set in a holocrystalline or variably glassy groundmass of interlocked feldspar laths and granular clinopyroxene and iron oxides. Uppermost flows from the wells UNIO-50683 (map no. 17), UNIO-50687 (map no. 18), and City of Imbler well UNIO-208 (Beeson, unpublished data) show a range of compositions from 55.17 to 57.34 weight percent SiO_2, 12.85 to 13.57 weight percent Al_2O_3, 2.30 to 2.43 weight percent K_2O, and 0.596 to 0.626 weight percent P_2O_5. Flows exposed in the Imbler quadrangle display normal remanent magnetic polarity and belong to the N2 magnetostratigraphic unit of Reidel and others (1989). Relatively high P_2O_5 and TiO_2 contents indicate a possible correlation of the uppermost flows in the wells UNIO-208 and UNIO-50687 with the N2 Indian Rock chemical type of Ferns and Madin (1999). Reidel and others (1989) consider the immediately underlying flows in the well UNIO-208 to be correlative with their Winter Water chemical type

Tcgv **Mafic hydrovolcanic deposits (middle Miocene)**—Bedded brown, yellowish-brown, or orangish-brown basaltic scoria and cinder deposits. Unit discontinuously crops out in the northeast part of the quadrangle, where it underlies thin olivine basalt pillow lavas of Glass Hill (unit Tpgb). Unit Tcgv consists of clast-supported breccia made up of dark-gray to black, finely vesiculated lapilli as much as 3 cm in diameter and set in a matrix of orange palagonite glass. Individual lapilli are fine grained and sparsely plagioclase phyric. In the Cricket Flat quadrangle to the northeast, unit covers the flanks of, and is interpreted to be related to, a north-northwest-trending ridge that is capped by as much as 70 m of black, glassy welded spatter. The spatter contains 56.26 weight percent SiO_2, 13.73 weight percent Al_2O_3, 2.38 weight percent TiO_2, and 0.40 weight percent P_2O_5 and is tentatively correlated with the N2 Winter Water chemical type of the Grande Ronde Basalt (Reidel and others, 1989)

Tci **Imnaha Basalt (middle and lower Miocene)** (shown in cross section only)—Inferred to underlie Mount Harris, from mapping by McConnell and others (2002) and Shubat (1979) along the Minam River to the east. Unit is largely made up of coarse-grained plagioclase and olivine phyric basalts

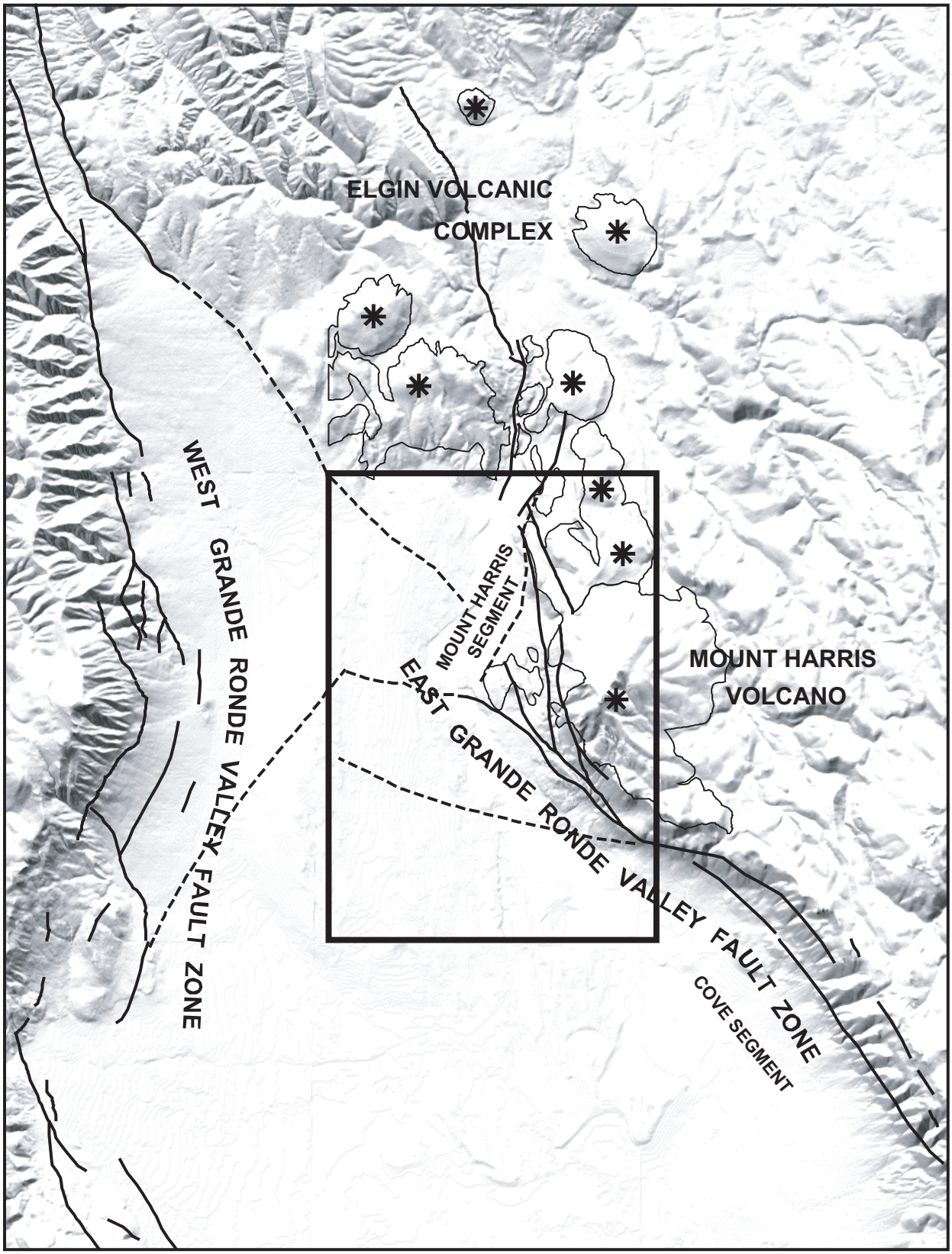

Figure 6. Major geologic features located in the Imbler quadrangle and the surrounding northern end of the Grande Ronde Valley include the Mount Harris volcano, the Elgin volcanic complex, the West Grande Ronde Valley fault zone, and the East Grande Ronde Valley fault zone. Dashed lines represent approximate location of major buried faults as inferred from water-well logs.

GEOMAGNETICS

Ground-based geomagnetic data were collected in the valley floor over 30 km² between Imbler and Alicel. The data were collected with a Geometrics G-856 portable magnetometer over a three-week period from February to March, 1999. Data were collected at paced 25-m intervals on east-west and north-south traverses across agricultural lands. Raw data were plotted, and deviations from 55,000 gammas were contoured by means of the Vertical Mapper software package. Contours and traverse lines are shown in Figure 7 (on map sheet). No diurnal corrections on the raw data were made. Power supply problems with the magnetometer terminated the survey after some 2,400 data points had been collected. We undertook the ground magnetic survey to see whether the thickness of the sedimentary fill correlated with total magnetic field strength. The magnetic highs and lows imaged south of Imbler do not correlate with observed thickness of the sedimentary section as based on water-well drill logs. Two traverses near the 320-m-thick sedimentary section measured at the well UNIO-50687 imaged a broad relative magnetic low (uncorrected 54,700 gammas), while two traverses near the 140-m-thick sedimentary section measured in the well UNIO-50833 imaged a broad relative magnetic low (uncorrected 54,800 gammas). The broad relative magnetic high (uncorrected 55,000 gammas) imaged near Janson Lane is penetrated by well UNIO-275, whose well log indicates a 270-m-thick section of sediments.

Buried faults may be imaged by areas with relatively sharp magnetic gradients. The most extreme gradients (10 gammas/meter) occur at the foot of Mount Harris along the east edge of the survey. These relatively high gradient zones correspond to a series of north-trending faults at the foot of Mount Harris.

STRUCTURE

The modern Grande Ronde Valley is best described as a pull-apart basin whose eastern margin is marked by down-to-the-west faults (Gehrels, 1981; White, 1981; Mann and Meyer, 1993) with as much as 350 m of vertical displacement along individual fault strands. The Imbler quadrangle covers the northeast margin of the valley and encompasses the transition zone between the northern and eastern valley margins. The northern valley margin is marked by a southeast-dipping homocline along which the top of the Powder River Volcanic Field plunges from the surface in the north end of the quadrangle to 135 m at Imbler. The northeast margin of the Grande Ronde Valley is marked by a closely spaced series of short-strike-length faults that separate the valley proper from the northwest-dipping homocline upon which Mount Harris sits. These faults form the Mount Harris fault zone (including the Mount Harris fault of White, 1981), which is considered by Simpson and others (1993) to be a segment of the larger East Grande Ronde Valley fault zone. The faults form a scissors zone along which the dominant down-to-the-west sense of displacement in the Imbler quadrangle changes to a dominant down-to-the-east sense of motion in the Elgin quadrangle to the north. Apparent lateral displacement of Glass Hill dacite (unit Tpgd) along the base of Mount Harris may indicate a right-lateral oblique-slip component at the south margin of the Mount Harris fault zone. The Mount Harris fault zone terminates in the large landslide complex at Grays Corner, where the zone is cut off on the south by the west-northwest-trending Cove segment of the East Grande Ronde Valley fault zone (Simpson and others, 1993; Personius, 1998). Linear ridges and bordering closed depressions in the landslide mass are interpreted as fault scarps that have been overrun by the debris flow rather than fault escarpments. Although the landslides cover a faulted surface, landslide surfaces do not appear to be offset by faulting (Personius, 1998).

The Cove segment of the East Grande Ronde Valley fault zone extends for nearly 20 km along the faceted spurs that mark the prominent eastern escarpment of the Grande Ronde Valley. The surface of the upthrown block on the east side of the East Grande Ronde Valley fault zone dips to the north-northwest, forming a topographic ramp that dives beneath the Mount Harris volcano. The Cove segment enters the Imbler quadrangle

from the southeast and cuts off the south end of the Mount Harris segment. Water-well logs indicate at least 340 m of down-to-the-south displacement where the fault trace projects beneath surficial units between the UNIO-50683 well and dacite exposures in the valley. Apparent down-to-the-south displacements manifested by 150- to 200-m increases in the depths to volcanic units in water wells south of Imbler suggest that strands of the East Grande Ronde Valley fault zone may continue westward beneath Sand Ridge. Cumulative down-to-the-south apparent displacement as measured by offsets in the top of the Grande Ronde Basalt is 500 m between the UNIO-208 and UNIO-50684 wells.

GEOLOGIC HISTORY

The Imbler quadrangle provides a record of 17 million years of continental volcanism and associated tectonism. Evolution of the Grande Ronde Valley at Imbler passed through three developmental stages: starting with widespread eruption of the Columbia River flood basalts, followed by eruptions forming small calc-alkalic and alkalic volcanoes in the Powder River Volcanic Field, and culminating with the large-scale faulting that has resulted in the modern valley. Columbia River Basalt Group volcanism began at about 17 Ma with eruption of Imnaha Basalt lavas (Baksi, 1989). Exposed in the Minam River Canyon 15 km to the east; flows of Imnaha Basalt flowed north and west from dike complexes to the southeast (McConnell and others, 2002), eventually covering more than 50,000 km^2 of Oregon, Idaho, and Washington with 9,500 km^3 of lava (Tolan and others, 1989). At about 16.5 Ma, even more massive amounts of flood basalts began erupting from vents in eastern Oregon, Washington, and western Idaho, producing as much as 150,000 km^3 of Grande Ronde Basalt (Tolan and others, 1989) over the next one million years. These massive eruptions resulted in a 700- to 800-m-thick blanket of stacked lava flows that would serve as the platform upon which younger Powder River Volcanic Field volcanoes would be built. The flood basalt platform is made up of tholeiitic (iron-rich) lavas characterized by low levels of alumina (typically less than 14 weight percent Al_2O_3).

Eruptions began in the Powder River Volcanic Field at about 14.5 Ma. Although extensive, the amount of lava erupted (estimated at about 400 km^3) was much smaller than earlier Columbia River Basalt Group eruptions. First lavas erupted were olivine basalts that followed channels entering into the quadrangle from the south. At about 13 Ma, high-silica andesite flows (>60 weight percent SiO_2) were erupted from a vent or vents south of the Imbler quadrangle, covering much of the southern Grande Ronde Valley area with a thick sheet of high-silica andesite. Basaltic andesite and andesite lavas, characterized by alumina levels of >16 weight percent Al_2O_3, then were erupted from along the axis of the ancestral Grande Ronde Valley, forming an sheet of stacked lava flows that are presently confined to the modern valley floor. Eruption of dacite and high-silica andesite flows began at about the same time, forming a 600-m-high volcano at Mount Harris.

Last eruptions at Mount Harris were about 11.9 Ma, with emplacement of a central dacite plug. Style of volcanism changed at about 10 Ma with small eruptions of alkalic lavas along the northern margin of the Imbler quadrangle that formed a number of small (<5 km^2) shield volcanoes between Imbler and Elgin. An unusually mafic lava (the Bell-tone basanite) was erupted at about this same time from a vent southeast of Mount Harris (McConnell and others, 2002), flowed down channels skirting the foot of the Mount Harris volcano, and moved toward the northeast corner of the quadrangle. Lavas erupted at this time are characterized by unusually high levels of strontium (>1,000 ppm Sr), and many of them contain hornblende crystals. Total volume of these later alkalic lavas is very small (estimated at <5 km^3) in comparison to the earlier calc-alkalic Powder River eruptions.

The Grande Ronde Valley began developing as a structural, fault-bounded basin following eruption of the Elgin volcanic rocks at about 10 Ma, in response to regional uplift and deformation of the Blue Mountains. By 8 Ma, the Grande Ronde Valley was actively subsiding, forming a catch basin for air-fall tuffs and fine-grained silts. Morphologic similarities between ~8 Ma

fish fossils in the Grande Ronde Valley and Ringold Formation fish fossils in the Pasco Basin to the northwest (Van Tassell and others, 2001) suggest a northwest outlet to the Grande Ronde Valley at that time. From that time to the present, the floor of the valley at Imbler has been settling unevenly; progressively tilting to the south, as the basin floor fragmented along buried faults. In response to climate and topographic changes, the valley at Imbler has been at different times a marshland with shallow, warm water ponds; a shallow to moderately deep lake system; and a windswept dune field.

GEOLOGIC HAZARDS

Debris-flow avalanches, possibly triggered by earthquakes, make up the most visible geologic hazard in the Imbler quadrangle. These avalanches occur when rock cliffs collapse and send debris cascading down the mountainside. Greatest potential for catastrophic debris flows exists downslope of places where high cliffs of dacite and andesite crop out high above the valley floor along the southwest flank of Mount Harris. Large landslide deposits on the southwest flank of Mount Harris are evidence of old collapses upslope of Grays Corner. Chances for future debris flows reaching the valley floor are somewhat lessened due to the formation of a catchment basin above the Mount Harris Loop Road. Although steep cliff faces can fail at any time without any apparent cause, movement along the East Grande Ronde Valley fault zone could potentially trigger future debris flows.

The large landslides in the southwest part of the Imbler quadrangle do not appear en masse to be of recent origin. Slide surfaces are somewhat stream dissected and, in places, mantled by alluvial fan and wind-blown ash deposits. Although linear topographic features on the slide surface above Grays Corner appear to be segments of the East Grande Ronde Valley fault zone, it is not clear whether the slide surface is actually offset by faults or whether the slide has ramped down over preexisting fault scarps.

The seismic threat presented to the Imbler area by the East Grande Ronde Valley fault zone cannot be determined at the present time. Most recent work by Geomatrix Consultants, Inc. (1989; 1995), and Personius (1998) has indicated that the West Grande Ronde Valley fault zone has been more active in the recent past than the East Grande Ronde Valley fault zone. Although Personius (1998), and Simpson and others (1993) have identified Holocene features along the East Grande Ronde Valley fault zone, more compelling evidence for Holocene ruptures can be found along the active West Grande Ronde Valley fault zone (Geomatrix Consultants, Inc., 1989, 1995; Personius, 1998; Ferns and others, 2001). Reasonable earthquake risk assessments for the Imbler quadrangle should be based on the premise that the West Grande Ronde Valley fault zone is more likely to generate a sizeable earthquake in the future. Currently the West Grande Ronde Valley fault zone is viewed as being capable of generating a maximum credible earthquake of magnitude 7 (Simpson and others, 1993).

GEOLOGIC RESOURCES

Aggregate in the form of crushed rock is the only mineral resource found in the quadrangle. Platy Powder River Volcanic Field flows such as dacite and andesite are locally crushed and used as aggregate. Blocky varieties of dacite may be suitable for use as coarse for rip rap.

Nearly all deep (>500 m) flowing wells in the Grande Ronde Valley yield water sufficiently warm enough to be considered as low-temperature (20°–30°C) geothermal aquifers (Brown and others, 1980). Records from irrigation and municipal wells drilled to date indicate that significant flows of water (>1,000 gpm) are nearly always encountered only after entering the Grande Ronde Basalt. To date, the overlying Powder River Volcanic Field has not yielded appreciable amounts of water. Warmest waters are encountered when irriga-

tion wells penetrate the Grande Ronde Basalt at depths greater than 800 m. The well UNIO-50687 encountered artesian flow of 43°C water in Grande Ronde Basalt flows at a depth of approximately 840 m. This well penetrated 350 m of Quaternary and Tertiary sediments and 370 m of Powder River Volcanic Field lavas before entering the Grande Ronde Basalt. A second deep well (UNIO-50684) first encountered an artesian flow of 32°C water in Powder River Volcanic Field lavas at a depth of approximately 640 m. This well penetrated about 580 m of sediment before entering Powder River Volcanic Field lavas. Significant artesian flow of warmer water (approximately 42°C) was encountered after penetrating into the underlying Grande Ronde Basalt at a depth of about 830 m.

ANALYTICAL METHODS

Mapping was supplemented with XRF major and trace-element geochemistry and $^{40}Ar/^{39}Ar$ radiometric age determinations. Table 1 lists the age determinations for selected samples, and Table 2 lists the geochemical analyses.

Rock-chip and water-well cuttings collected by Oregon Department of Geology and Mineral Industries staff were examined for alteration and weathering. Suitable samples were submitted to the Washington State University GeoAnalytical Laboratory (WSU) at Pullman, Washington. Crushed samples were fused to glass beads using lithium tetraborate as a flux. Samples were analyzed for major and selected trace element concentrations using Washington State University GeoAnalytical Laboratory's automatic Rigaku 3370 spectrometer. Each element analysis is fully corrected for line interference and matrix effects. Results have been normal ized on a volatile-free basis and recalculated with total iron expressed as FeO.

Felsic volcanic ash that occurred in concentrated amounts in the valley-fill sequence in well cuttings was examined petrographically to determine if the sample appeared unaltered and unweathered. Suitable samples of isotropic glass and euhedral phenocrysts were separated into pure concentrates using heavy liquids. Glass and sanidine separates were irradiated and processed for $^{40}Ar/^{39}Ar$ radiometric age determinations, incrementally fused using a coherent 6W Ar-ion laser, and argon isotope ratios measured on a VG3600 mass spectrometer at the University of Alaska Fairbanks Geochronology Lab. Sample ages were calculated using the Bern 4B biotite standard (17.25 Ma), and standard deviations are reported to 1 σ.

Aphyric andesite or dacite and olivine phyric basanite lava rocks were prepared for whole-rock $^{40}Ar/^{39}Ar$ radiometric age determinations. Large, >1-kg, hand samples were coarsely crushed, and any weathering or altered pieces removed.

For felsic rocks, an ~100-g split was then further crushed and a final split sent for irradiation and processing. The irradiated sample was incrementally fused using a double vacuum resistance furnace, and the argon isotope ratios measured on a MAP 215-50 mass spectrometer at the Nevada Isotope Geochronology Lab, University of Nevada. Sample ages were calculated using the Fish Canyon Tuff sanidine standard (27.9 Ma), and data are reported at the confidence level of 1 σ (standard deviation).

For phyric samples, an ~100 g split was then further crushed and a final split sent for irradiation and processing. The argon isotopes in the irradiated sample were measured on a MAP 215 rare-gas mass spectrometer with on-line, double-vacuum furnace extraction system at the Oceanography Dept. of the Oregon State University, Corvallis, Oregon. Data are reported at the confidence level of 1 σ (standard deviation).

ACKNOWLEDGMENTS

We sincerely thank the many landowners who allowed access across their property. We especially thank the Bingaman clan, including Elwyn, Greg, Howard, Russell, Ross, and Shawn. The Bingaman deep water wells proved to be a bonanza of geologic data. We also thank the Cuthbert, Delint, Royes, Shaw, and Wagner families. Special thanks are given to Waldo Lowe and his drilling assistants whose drilling and sampling expertise has greatly expanded our understanding of the strata beneath the Grande Ronde Valley. We also thank Dr. Marvin Beeson, Portland State University, who first developed the framework of the subsurface volcanic stratigraphy using geochemical analyses of well cuttings. Special thanks are given to the Grande Ronde Model Watershed Board and Boise Cascade Corporation for supporting our efforts to secure funding for this study. Thanks are also given to Boise Cascade for providing airphotos as well as key access to their timbered lands on Mount Harris. We also like to thank James G. Evans, U. S. Geological Survey and Ronald P. Geitgey, Oregon Department of Geology and Mineral Industries for their constructive reviews.

REFERENCES CITED

Bailey, D.E., 1990, Geochemistry and petrogenesis of Miocene volcanic rocks in the Powder River volcanic field, northeastern Oregon: Pullman, Wash., Washington State University doctoral dissertation, 341 p.

Baksi, A.K., 1989, Reevaluation of the timing and duration of extrusion of the Imnaha, Picture Gorge, and Grande Ronde Basalts, Columbia River Basalt Group, *in* Reidel, S.P., and Hooper, P.R., eds., Volcanism and tectonism in the Columbia River flood-basalt province: Geological Society of America Special Paper 239, p. 105–112.

Barrash, W., Bond, J.G., Kauffman, J.D., Venkatakrishnan, R., 1980, Geology of the La Grande area, Oregon: Oregon Department of Geology and Mineral Industries Special Paper 6, 47 p.

Brown, D.E., Black, G.L., McLean, G.D., 1980, Preliminary geology and geothermal resource potential of the Craig Mountain-Cove area, Oregon: Oregon Department of Geology and Mineral Industries Open File Report O–80–4, 68 p.

Ferns, M.L., and Madin, I.P, 1999, Geologic map of the Summerville quadrangle, Union County, Oregon: Oregon Department of Geology and Mineral Industries Geological Map Series GMS-111, scale 1:24,000.

Ferns, M.L., Madin, I.P., and Taubeneck, W.H., 2001, Reconnaissance geologic map of the La Grande 30x60 minute quadrangle, Baker, Grant, Umatilla, and Union Counties, Oregon: Oregon Department of Geology and Mineral Industries Reconnaissance Map Series RMS-1, scale 1:100,000.

Ferns, M.L., Madin, I.P., McConnell, V.S., and Johnson, J. A., in preparation, Surface and subsurface geology of the southern Grande Ronde Valley and lower Catherine Creek drainage, Union County, Oregon: Implications for Groundwater Flow: Oregon Department of Geology and Mineral Industries Open-File Report.

Fiebelkorn, R.B., Walker, G.W., MacLeod, N.S., McKee, E.H., and Smith, J.G., 1983, Index to K-Ar [age] determinations for the State of Oregon: Isochron/West, no. 37, p. 3–60. (also 1982, USGS OFR 82–596)

Gehrels, G.E., 1981, The geology of the western half of the La Grande Basin, northeastern Oregon: Los Angeles, Calif., University of Southern California master's thesis, 97 p.

Geomatrix Consultants, 1989, Final seimotectonic evaluation for Mann Creek dam site (Idaho) and Mason Creek dam site (Oregon): Unpublished report prepared for U.S. Bureau of Reclamation, 118 p.

Geomatrix Consultants, Inc., 1995, Seismic design mapping, State of Oregon: Final report to Oregon Department of Transportation, Project no. 2442, var. pag.

Hampton, E.R., and Brown, S.G., 1964, Geology and groundwater resources of the upper Grande Ronde River basin, Union County, Oregon: U.S. Geological Survey Water-Supply Paper 1597, 99 p.

Hooper, P.R., and Swanson, D.A., 1990, The Columbia River Basalt Group and associated volcanic rocks of the Blue Mountains province, chap. 4 *of* Walker, G.W., ed., Geology of the Blue Mountains region of Oregon, Idaho, and Washington: Cenozoic geology of the Blue Mountains region: U.S. Geological Survey Professional Paper 1437, p. 63–99.

Kienle, C.F., Jr., Hamill, M.L., and Clayton, D.N., 1979, Geological reconnaissance of the Wallula Gap, Washington-Blue Mountains-La Grande, Oregon, region: Unpublished report prepared for the

Washingon Public Power Supply System by Shannon and Wilson, Inc., Contract No. 44013, C.O. No 38, 58 p.
Kuno, H., 1968, Differentiation of basalt magmas, *in* Hess, H.H., and Poldevaart, Arie., eds., Basalts—The Poldevaart treatise on rocks of basaltic composition: New York, John Wiley, v. 2, p. 624–688.
Le Maitre, R.W., Bateman, P., Dudek, A., Keller, J., Lemeyre, J., Le Bas, M.J., Sabine, P.A., Schmid, R., Sorensen, H., Streckeisen, A., Wooley, A.R., and Zanettin, B., 1989, A classification of igneous rocks and glossary of terms: Oxford, Blackwell, 193 p.
Mann, G.M., and Meyer, C.E., 1993, Late Cenozoic structure and correlations to seismicity along the Olympic-Wallowa lineament, northwest United States: Geological Society of America Bulletin, v. 105, p. 853–871.
McConnell, V.S., Betteridge, I.P., and Ferns, M.L., 2002, Geologic map of the Mount Fanny and Little Catherine Creek quadrangles, Union and Wallowa Counties, Oregon: Oregon Department of Geology and Mineral Industries Geological Map Series GMS–115, scale 1:24,000.
Miyashiro, A., 1974, Volcanic rock series in island arcs and active continental margins: American Journal of Science, v. 274, p. 321–355.
Personius, S.F., 1998, Surficial geology and neotectonics of selected areas of western Idaho and northeastern Oregon: U.S. Geological Survey Open-File Report 98-771, 26 p.
Reidel, S.P., Beeson, M.H., Tolan, T.L., and Lindsey, K.A., 1996, The age of La Grande basin (LGB), northeast Oregon: New evidence for middle Miocene deformation and basin formation [abs.]: Geological Society of America Abstracts with Programs, v. 28, no 5, p. 104.
Reidel, S.P., Tolan, T.L., Hooper, P.R., Beeson, M.H., Fecht, K.R., Bentley, R.D., and Anderson, J.L., 1989, The Grande Ronde Basalt, Columbia River Basalt Group; stratigraphic descriptions and correlations in Washington, Oregon, and Idaho, *in* Reidel, S.P., and Hooper, P.R., eds., Volcanism and tectonism in the Columbia River flood-basalt province: Geological Society of America Special Paper 239, p. 21–53.
Shubat, M.A., 1979, Stratigraphy, petrochemistry, petrography, and structural geology of the Columbia River basalt in the Minam-Wallowa Rivers area, northeast Oregon: Pullman, Wash., Washington State University master's thesis, 156 p.
Simpson, G.D., Hemphill-Haley, M.A., Wong, I.G., Bott, J.D.J., Silva, W.J., and Lettis, W.R., 1993, Seismotectonic evaluation, Unity Dam, Burnt River Project—Thief Valley Dam, Baker Project, northeastern Oregon: Final report prepared for U.S. Bureau of Reclamation by William Lettis & Associates and Woodward-Clyde Federal Services, 167 p.
Tolan, T.L., Reidel, S.P., Beeson, M.H., Anderson, J.L., Fecht, K.R., and Swanson, D.A., 1989, Revisions to the estimates of the areal extent and volume of the Columbia River Basalt Group, *in* Reidel, S.P., and Hooper, P.R., eds., Volcanism and tectonism in the Columbia River flood-basalt province: Geological Society of America Special Paper 239, p. 1–20.
Van Tassell, J., 1997, Cyclostratigraphy of the Grande Ronde graben, NE Oregon [abs.]: Geological Society of America Abstracts with Programs, v. 29, no. 5, p. 71.
Van Tassell, J., Ferns, M.L., McConnell, V.S., and Smith, G.R., 2001, The mid-Pliocene Imbler fish fossils, Grande Ronde Valley, Union County, Oregon, and the connection between Lake Idaho and the Columbia River: Oregon Geology, v. 63, no. 3, p. 77–96.
Walker, G.W., 1979, Reconnaissance geologic map of the Oregon part of the Grangeville quadrangle, Baker, Union, Umatilla, and Wallowa Counties, Oregon: U.S. Geological Survey Miscellaneous Investigations Series Map I–1116, scale 1:250,000.
White, R.R., 1981, Structural geology of the eastern half of the La Grande basin, northeastern Oregon: Los Angeles, Calif., University of Southern California master's thesis, 133 p.

Table 2. Analyses of major and trace elements from samples and well cuttings collected in the Imbler, Summerville, and Gassett ses normalized to 100 percent on a volatile-free basis with all iron calculated as FeO. Map numbers identify samples from the (Layout extends to opposite page ➤ and table is continued on following pages 20-21)

Sample no.	Map no.	Longitude	Latitude	¼	¼	Sec.	T. (S)	R. (E)	Elev. (ft)	Map unit	Lithology	SiO_2	Al_2O_3	TiO_2	FeO*	MnO
Imbler quadrangle																
98MAD169	10	-117.904944	45.441271	NW	NW	35	1	39	4,270	Tgha	Andesite	61.59	16.56	1.105	5.81	0.11
98MAD171	14	-117.907437	45.438217	NW	NW	35	1	39	3,840	Tpgd	Dacite	65.17	16.26	0.739	4.34	0.07
98MAD173	13	-117.906806	45.438801	NW	NW	35	1	39	3,950	Tgha	Andesite	61.11	16.57	1.168	5.88	0.11
98MAD174	12	-117.905901	45.439440	NW	NW	35	1	39	4,080	Tgha	Andesite	61.31	16.56	1.125	5.89	0.11
98MAD175	11	-117.905341	45.439843	NW	NW	35	1	39	4,180	Tgha	Andesite	61.46	16.56	1.102	5.89	0.11
98MAD177	9	-117.901194	45.440262	NE	NW	35	1	39	4,480	Tghd	Dacite	64.95	16.78	0.776	4.46	0.07
98MAD177R	9	-117.901194	45.440262	NE	NW	35	1	39	4,480	Tghd	Dacite	64.94	16.79	0.777	4.49	0.07
98MAD179	6	-117.895647	45.444634	SE	SE	26	1	39	5,200	Tghp	Dacite	67.59	16.66	0.509	3.02	0.07
98MAD198	3	-117.921983	45.481945	SE	NW	15	1	39	2,840	Tghd	Dacite	64.02	17.02	0.803	4.50	0.06
99-LG-41	8	-117.897300	45.442300	SW	SE	26	1	39	5,020	Tghd	Dacite	67.31	16.47	0.529	3.50	0.05
99-LG-41R	8	-117.897300	45.442300	SW	SE	26	1	39	5,020	Tghd	Dacite	67.33	16.49	0.535	3.51	0.05
99-LG-43	4	-117.902000	45.447200	NE	SW	26	1	39	4,580	Tghd	Dacite	63.00	16.43	0.912	5.39	0.10
99-LG-59	5	-117.902640	45.444080	SW	SE	26	1	39	4,620	Tghp	Dacite	66.64	16.48	0.561	3.41	0.05
99-LG-59R	5	-117.902640	45.444080	SW	SE	26	1	39	4,620	Tghp	Dacite	66.62	16.46	0.564	3.55	0.05
99-LG-76	1	-117.897810	45.496650	NW	NE	11	1	39	3,440	Tpea	Andesite	60.21	17.83	0.817	5.42	0.09
99-LG-78	2	-117.894750	45.478220	NW	SE	14	1	39	3,820	Tpea	Andesite	60.67	18.43	0.686	5.14	0.09
99-LG-79	16	-117.896260	45.426870	NE	NE	2	2	39	4,420	Tghi	Dacite	63.54	16.39	0.886	4.67	0.09
99-LG-82	15	-117.919460	45.442280	SW	SE	27	1	39	2,900	Tpgd	Dacite	64.82	16.29	0.737	4.47	0.09
99-VLG-16	7	-117.886100	45.445200	SW	SW	25	1	39	5,030	Tghp	Dacite	68.95	16.66	0.428	2.91	0.03
IM-1-1011	17	-117.934000	45.433500	NE	SE	33	1	39	1,679	Tpgd	Dacite	63.40	16.65	0.800	4.58	0.07
IM-1-1137	17	-117.934000	45.433500	NE	SE	33	1	39	1,553	Tpga	Andesite	58.15	17.62	1.212	6.91	0.14
IM-1-1931	17	-117.934000	45.433500	NE	SE	33	1	39	759	Tcgn2	Ferrobasaltic andesite	55.40	13.20	2.361	13.61	0.24
IM-1-2106	17	-117.934000	45.433500	NE	SE	33	1	39	584	Tcgn2	Basalt	51.90	13.91	2.199	15.04	0.23
IM-1-2144	17	-117.934000	45.433500	NE	SE	33	1	39	546	Tcgn2	Basaltic andesite	53.58	13.55	2.288	14.08	0.22
IM-1-2357	17	-117.934000	45.433500	NE	SE	33	1	39	333	Tcgn2	Ferrobasaltic andesite	56.02	13.69	2.105	12.15	0.20
IM-1-2507	17	-117.934000	45.433500	NE	SE	33	1	39	183	Tcgn2	Andesite	53.63	14.47	1.947	12.08	0.23
SV51-1132	18	-117.967000	45.409400	C	NW	8	2	39	1,605	Tpgd	Dacite	64.39	16.68	0.695	4.38	0.09
SV51-1198	18	-117.967000	45.409400	C	NW	8	2	39	1,539	Tpgd	Dacite	65.01	16.61	0.722	4.22	0.09
SV51-1274	18	-117.967000	45.409400	C	NW	8	2	39	1,463	Tpgd	Dacite	63.58	16.89	0.721	4.52	0.09
SV51-1365	18	-117.967000	45.409400	C	NW	8	2	39	1,372	Tpgd	Dacite	63.45	16.77	0.712	4.58	0.08
SV51-1444	18	-117.967000	45.409400	C	NW	8	2	39	1,293	Tpgd	Dacite	63.60	16.84	0.721	4.59	0.09
SV51-1743	18	-117.967000	45.409400	C	NW	8	2	39	994	Tpga	Andesite	57.49	17.39	1.356	7.65	0.14
SV51-1832	18	-117.967000	45.409400	C	NW	8	2	39	905	Tpga	Andesite	57.29	17.26	1.321	7.86	0.15
SV51-1902	18	-117.967000	45.409400	C	NW	8	2	39	835	Tpga	Andesite	57.26	17.43	1.278	7.46	0.15
SV51-1971	18	-117.967000	45.409400	C	NW	8	2	39	766	Tpga	Andesite	56.53	17.24	1.311	7.80	0.15
SV51-2071	18	-117.967000	45.409400	C	NW	8	2	39	666	Tpgb	Basalt	50.81	17.25	1.839	10.38	0.17
SV51-2119	18	-117.967000	45.409400	C	NW	8	2	39	618	Tpga	Andesite	56.43	17.41	1.304	7.76	0.16
SV51-2222	18	-117.967000	45.409400	C	NW	8	2	39	515	Tpga	Andesite	56.12	17.36	1.317	8.05	0.16
SV51-2329	18	-117.967000	45.409400	C	NW	8	2	39	406	Tpga	Andesite	56.25	17.70	1.361	7.75	0.16
SV51-2349	18	-117.967000	45.409400	C	NW	8	2	39	386	Tpga	Andesite	56.28	17.64	1.362	7.78	0.18
SV51-2382	18	-117.967000	45.409400	C	NW	8	2	39	353	Tpga	Basaltic andesite	54.36	17.12	1.783	10.61	0.20
SV51-2429	18	-117.967000	45.409400	C	NW	8	2	39	313	Tcgn2	Ferrobasaltic andesite	57.34	13.58	2.438	12.77	0.15

Bluff quadrangles, Union County, Oregon. Major elements in percent, trace elements in parts per million (ppm). XRF analy-Imbler quadrangle only. Samples analyzed by the Washington State University GeoAnalytical Laboratory at Pullman, Wash.

CaO	MgO	K_2O	Na_2O	P_2O_5	Ni	Cr	Sc	V	Ba	Rb	Sr	Zr	Y	Nb	Ga	Cu	Zn	Pb	La	Ce	Th
5.70	2.78	1.89	4.01	0.449	23	41	15	117	664	24	544	181	22	18.6	17	33	76	9	30	36	3
5.14	1.89	1.66	4.41	0.327	14	35	13	93	603	21	654	160	15	8.6	20	18	75	7	33	55	4
5.73	2.96	2.11	3.90	0.463	27	48	11	135	646	22	546	181	22	19.2	20	38	78	4	29	48	4
5.71	2.89	2.11	3.85	0.455	25	47	14	133	664	24	542	182	22	18.0	21	32	78	5	30	47	3
5.67	2.81	2.07	3.88	0.447	24	45	18	135	644	26	536	181	21	18.7	21	33	79	4	26	47	4
5.01	1.52	1.78	4.31	0.341	16	35	10	86	685	26	548	168	18	12.9	20	18	70	6	32	46	0
5.00	1.50	1.78	4.33	0.342	15	30	13	85	684	25	547	169	19	13.4	21	21	69	6	23	51	4
4.55	0.88	1.74	4.74	0.244	12	20	9	68	663	24	642	157	13	8.0	23	20	63	6	27	59	1
5.43	1.65	1.65	4.51	0.374	17	45	10	104	577	21	685	170	17	14.9	20	23	77	8	36	47	1
4.52	0.98	1.84	4.54	0.266	7	21	10	83	678	27	641	160	16	7.1	18	20	71	8	38	53	4
4.52	0.95	1.84	4.50	0.269	8	18	7	83	677	28	640	159	16	7.1	18	21	69	7	22	48	5
5.42	2.55	1.92	3.87	0.402	19	36	11	103	674	28	520	177	22	13.0	18	34	77	7	33	45	4
4.73	1.40	1.78	4.64	0.300	8	19	11	61	641	24	766	157	14	7.1	20	27	65	7	26	49	3
4.73	1.38	1.78	4.56	0.295	6	17	10	74	648	24	769	156	12	6.5	18	30	68	5	39	59	4
5.99	2.80	1.84	4.59	0.418	39	47	12	117	926	15	1,068	119	15	6.4	22	46	77	8	27	49	2
6.23	2.33	1.44	4.63	0.362	26	32	11	104	824	12	1,082	102	13	4.1	20	54	78	8	30	47	1
5.39	2.07	1.87	4.61	0.493	15	40	11	100	698	22	1,021	165	15	12.3	19	26	83	8	34	68	3
5.19	2.08	1.61	4.37	0.328	12	34	7	98	597	20	655	155	16	7.7	18	21	80	8	22	63	1
4.01	0.55	1.80	4.45	0.199	5	11	3	50	764	25	618	150	10	5.9	17	26	57	10	24	53	5
5.37	2.31	1.78	4.61	0.432	28	51	15	88	637	22	916	176	15	13.1	22	27	74	7	28	45	2
6.59	3.11	1.65	4.01	0.597	13	29	19	137	651	23	707	179	24	19.1	21	35	85	8	43	55	1
6.69	2.94	1.65	3.31	0.601	0	14	29	261	761	44	314	201	44	17.3	25	5	143	9	35	65	5
8.24	4.25	0.72	3.11	0.404	0	20	36	400	513	17	350	171	37	13.6	21	21	132	5	18	40	5
7.65	3.73	1.43	3.08	0.392	0	20	30	433	625	39	315	175	38	14.2	22	21	128	7	22	37	5
7.00	3.47	1.81	3.21	0.355	0	22	31	367	756	52	306	176	37	14.7	21	16	121	8	25	53	8
8.32	4.66	1.21	3.09	0.366	11	37	32	334	646	36	314	170	38	14.1	22	42	116	7	22	48	7
5.32	2.18	1.75	4.17	0.347	20	38	14	96	639	24	700	164	16	12.9	20	15	74	6	38	46	3
5.02	1.82	1.77	4.38	0.371	23	35	14	95	637	23	711	169	15	13.6	17	12	74	6	17	61	1
5.49	2.61	1.78	3.99	0.336	38	60	13	91	534	23	682	165	14	12.3	21	14	79	7	31	47	3
5.40	2.85	1.64	4.19	0.332	37	59	16	100	540	22	675	163	15	11.4	20	16	74	6	28	51	3
5.40	2.56	1.60	4.26	0.335	40	60	7	99	543	20	682	164	15	12.5	19	20	82	3	35	50	4
6.52	3.01	1.59	4.20	0.649	17	39	18	163	618	19	648	195	26	24.2	22	28	96	5	35	55	3
6.58	3.32	1.50	4.09	0.641	18	43	19	145	601	16	640	192	26	23.5	18	28	92	4	24	57	3
6.57	3.52	1.53	4.17	0.637	18	46	17	153	615	17	639	192	26	22.8	19	33	89	4	22	72	3
6.78	3.89	1.57	4.06	0.657	19	45	17	151	550	19	690	188	26	22.3	18	33	97	5	30	54	4
9.33	5.87	0.63	3.19	0.520	103	215	28	257	376	6	532	138	24	17.5	19	34	89	2	5	31	4
6.92	4.05	1.31	4.04	0.627	22	52	15	160	534	17	658	188	27	23.2	25	323	97	6	18	72	1
6.93	3.94	1.28	4.19	0.656	20	50	14	164	552	15	710	187	25	23.1	20	39	94	5	21	63	1
7.06	3.90	1.36	3.81	0.663	20	45	18	154	510	18	635	192	27	24.6	21	43	96	4	17	63	2
7.17	3.70	1.34	3.92	0.638	25	48	21	157	527	18	637	185	25	22.7	20	36	95	5	84	74	3
7.37	3.38	0.91	3.63	0.642	11	37	23	202	538	11	607	207	33	22.7	20	24	132	8	17	81	5
5.36	1.65	2.58	3.51	0.627	0	15	27	247	794	90	305	205	41	16.3	25	7	139	6	4	98	5

(Table continued on following pages)

Table 2. Continued

Sample no.	Map no.	Longitude	Latitude	¼	¼	Sec.	T. (S)	R. (E)	Elev. (ft)	Map unit	Lithology	SiO_2	Al_2O_3	TiO_2	FeO*	MnO
Summerville quadrangle																
98BI1502	-	-118.006000	45.399100	SW	SE	12	2	38	1,278	QTal	Rhyolite ash	71.15	17.90	0.321	2.29	0.19
98BI1553	-	-118.006000	45.399100	SW	SE	12	2	38	1,227	QTal	Rhyolite ash	72.69	16.08	0.342	2.31	0.10
98BI1916	-	-118.006000	45.399100	SW	SE	12	2	38	864	Tpga	Basaltic andesite	55.65	17.68	1.752	8.50	0.22
98BI1931	-	-118.006000	45.399100	SW	SE	12	2	38	849	Tpga	Andesite	56.19	17.26	1.732	8.32	0.18
98BI1960	-	-118.006000	45.399100	SW	SE	12	2	38	820	Tpga	Basaltic andesite	54.24	18.85	1.915	9.02	0.19
98BI2002	-	-118.006000	45.399100	SW	SE	12	2	38	778	Tpga	Basaltic andesite	53.99	18.29	1.895	9.03	0.21
98BI2072	-	-118.006000	45.399100	SW	SE	12	2	38	708	Tpga	Andesite	56.42	17.83	1.853	8.61	0.13
98BI2109	-	-118.006000	45.399100	SW	SE	12	2	38	671	Tpga	Basaltic andesite	54.82	17.83	1.800	9.48	0.20
98BI2164	-	-118.006000	45.399100	SW	SE	12	2	38	616	Tpga	Basaltic andesite	55.06	18.13	1.788	8.65	0.20
98BI2281	-	-118.006000	45.399100	SW	SE	12	2	38	499	Tpga	Basaltic andesite	54.39	18.86	1.498	8.33	0.18
98BI2329	-	-118.006000	45.399100	SW	SE	12	2	38	451	Tpga	Andesite	56.77	17.54	1.346	7.54	0.18
98BI2383	-	-118.006000	45.399100	SW	SE	12	2	38	397	Tpgb	Basalt	50.57	16.53	1.884	10.13	0.20
98-Bingaman	-	-118.006000	45.399100	SW	SE	12	2	38	1,030	Tpga	Basaltic andesite	55.83	19.70	1.834	13.36	0.15
98-BingamanR	-	-118.006000	45.399100	SW	SE	12	2	38	1,030	Tpga	Andesite	56.02	20.57	1.825	13.50	0.13
Gasset Bluff quadrangle																
99-LG-72	-	-117.872040	45.475430	NE	SE	13	1	39	3,600	Tpgh	Basanite	44.26	13.83	3.099	14.86	0.21

CaO	MgO	K_2O	Na_2O	P_2O_5	Ni	Cr	Sc	V	Ba	Rb	Sr	Zr	Y	Nb	Ga	Cu	Zn	Pb	La	Ce	Th
1.91	2.76	2.06	1.37	0.051	28	11	7	47	391	47	128	207	112	47.6	26	16	122	28	25	76	12
1.74	1.68	2.91	2.09	0.050	16	15	9	40	940	61	154	168	23	7.4	18	17	56	16	13	53	12
7.19	3.23	1.14	3.89	0.755	23	50	19	185	551	15	620	195	27	24.0	21	28	108	3	37	66	4
7.17	3.26	1.37	3.78	0.737	23	49	20	197	505	16	606	191	27	23.5	21	35	104	4	26	73	3
7.37	2.92	0.79	3.90	0.803	22	54	21	202	468	10	651	204	27	24.2	21	28	107	7	40	54	4
7.61	3.40	0.80	3.99	0.787	23	46	23	195	547	10	644	198	25	24.2	21	34	112	4	37	64	6
6.59	2.02	1.59	4.17	0.790	27	50	17	191	604	22	597	197	27	25.2	23	40	110	5	31	61	1
7.30	3.20	0.98	3.61	0.780	20	48	23	191	466	14	656	203	29	25.3	24	34	117	6	30	50	0
7.43	3.20	1.02	3.75	0.790	19	49	16	189	501	14	654	196	29	23.3	20	38	115	4	18	60	0
7.51	3.28	0.94	4.28	0.730	23	51	14	157	637	8	771	187	25	21.2	21	41	106	7	20	58	1
6.88	3.38	1.46	4.24	0.670	23	44	15	155	553	18	661	181	27	21.4	20	46	99	0	38	66	3
9.22	7.43	0.54	2.98	0.515	107	208	29	253	421	4	488	137	27	16.6	17	31	88	2	10	56	1
3.94	1.19	1.05	2.34	0.622	28	59	20	207	821	13	331	202	38	23.8	23	42	128	10	28	55	5
3.41	0.96	0.99	1.99	0.597	36	57	19	212	696	14	278	204	32	23.7	25	40	129	8	36	55	4
9.28	7.86	1.47	4.52	0.606	73	114	24	380	472	6	1,083	87	18	6.1	21	127	161	5	0	40	0

Table 3. Deep water wells in and adjacent to the Imbler quadrangle. Depth to Grande Ronde Basalt based on well-log interpretations.

Well name	Well owner	Total depth m (ft)	Depth to rocks of Powder River Volcanic Field m (ft)	Depth to Grande Ronde Basalt m (ft)	Reported yield (gal/min)	Artesian flow (gal/min)	Temperature °C (°F)
UNIO-208	City of Imbler	471 (1,544)	134 (441)	336 (1,102)	2,500	2,500	26 (78)
UNIO-271	Elwyn Bingaman	363 (1,190)	193 (632)	318 (1,044)	3,000	3,000	nd
UNIO-275	Creston Shaw	280 (920)	262 (858)	nd	3,180	3,180	27(80)
UNIO-2046	Elwyn Bingaman	549 (1,802)	360 (1,180)	433 (1,420)	494	494	29 (85)
UNIO-2047	Royes Farms	248 (815)	175 (575)	248 (815)	1,660	1,660	22 (71)
UNIO-50083	Russ Bingaman	773 (2,536)	344 (1,130)	588 (1,930)	700	0	33 (91)
UNIO-50452	Homer Case	218 (715)	nd	nd	1,850	0	13 (55)
UNIO-50684	Greg Bingaman	956 (3,138)	584 (1,916)	823 (2,700)	1,700	350	38 (101)
UNIO-50687	Creston Shaw	930 (3,050)	345 (1,132)	740 (2,429)	1,000	300	40 (104)
UNIO-50763	John Cuthbert	867 (2,844)	nd	nd	50	0	32 (90)
UNIO-50833	Ross Bingaman	581 (1,905)	126 (412)	372 (1,220)	2,000	2,000	nd